Materials Today Communications 23 (2020) 100912

Contents lists available at ScienceDirect

Materials Today Communications

journal homepage: www.elsevier.com/locate/mtcomm

# Development and characterization of single polymer composites prepared by compression molding of polyamide 6 empty microcapsules and novel woven textile structures

Shafagh. D. Tohidi[a,b,c,*], Nadya Dencheva[b], Zlatan Denchev[b], Ana Maria Rocha[c], Bernhard Engesser[d]

[a] CMEMS - UMinho, Department of Mechanical Engineering, University of Minho, Guimarães, Portugal
[b] IPC - Institute for Polymers and Composites, Department of Polymer Engineering, University of Minho, Guimarães, Portugal
[c] Center of Textile Science and Technology (2C2T), Department of Textile Engineering, University of Minho, Guimarães, Portugal
[d] Jakob Müller AG, Frick, Switzerland

ARTICLE INFO

*Keywords:*
Single polymer composite
Microcapsules
Polyamide 6
Woven reinforcements
Tensile properties
Impact properties
Transcrystallinity

ABSTRACT

In the present study, novel polyamide 6 based woven single polymer composites (WSPC) were developed by powder-coating of woven textile structures with polyamide 6 empty microcapsules (EMC) and subsequent compression molding. To synthesize EMC, activated anionic ring-opening polymerization of ε-caprolactam by solution/precipitation was applied. Stitched plain fabrics that are promising novel class of woven fabrics and two conventional woven patterns (plain and satin-5 harness) were used as textile reinforcements. The thermal and mechanical properties of all composites were characterized and related to the reinforcements´ morphology, fiber volume fraction and ply orientation. For better understanding of the bonding state at the matrix-fiber interface, stereo-optical microscopy and SEM image analysis by image processing were performed. The data obtained confirmed the existence of a transcrystalline layer (TCL) in the interface region. The mechanical behavior of the composites was related also to the PA6 polymorph content of the samples and their crystallinity indexes determined by wide-angle X-ray diffraction experiments.

## 1. Introduction

One of the main advantages of the thermoplastic composites is the possibility for their reprocessing when heated above a certain temperature [1]. Nowadays the environmental impact of conventional composites with glass- or carbon fiber reinforcements has become subject of studies for declining the man-made contamination. This stimulated the interests toward a novel class of composite materials denominated as “Single Polymer Composites” (SPC) [2]. The isotropic polymer matrix in SPC is reinforced with oriented 2D or 3D fibrous structures, all composite elements being made of the same polymer. Because of this chemical identity, better matrix/reinforcements interfacial bonding [3] and higher percentage of recyclability [1,4] can be anticipated. Exhaustive recent reviews on the SPC preparation, morphology, and mechanical behavior are available [2,5–10].

There exist usual techniques for SPC preparation, such as powder impregnation, hot compaction, overheating of fibers (partially melting), film-stacking, and co-extrusion [5,11–13]. In all of these cases the reinforcing material partially melts during the SPC consolidation, thus forming the isotropic matrix. At the same time, the inner part of the reinforcements should not melt and remain highly oriented. Widening the processing window is the main challenge for SPC preparation containing different reinforcement architectures [12,14–19].

Several studies are available describing the production and properties of polyamide 6 (PA6)-based SPC. Bhattacharyya et al. [20] combined two basic techniques such as hot compaction and film stacking used for the preparation of PA6 based SPC composed of melt-quenched PA6 film (matrix) in the presence of PA6 high tenacity filament (as reinforcement). All reinforcements were treated with $Sb_2O_3$ to improve the interfacial adhesion via trans-reactions. The processing window obtained was only 2 °C, however, the use of a catalyst caused an improvement on the tensile stiffness and strength by more than 30 % for the dry samples and by 8–20 % for the conditioned samples.

Gong et al. [15] investigated on the in situ activated anionic ring opening polymerization (AAROP) of ε -caprolactam (ECL) to prepare PA6-based SPC reinforced by PA6 plain weave fabric. The tensile

* Corresponding author at: the center for textile science and technology (2C2T), Department of Textile Engineering, University of Minho, Guimarães, Portugal.
*E-mail address:* shafagh.project@gmail.com (S.D. Tohidi).

https://doi.org/10.1016/j.mtcomm.2020.100912
Received 18 October 2019; Received in revised form 7 January 2020; Accepted 8 January 2020
Available online 09 January 2020

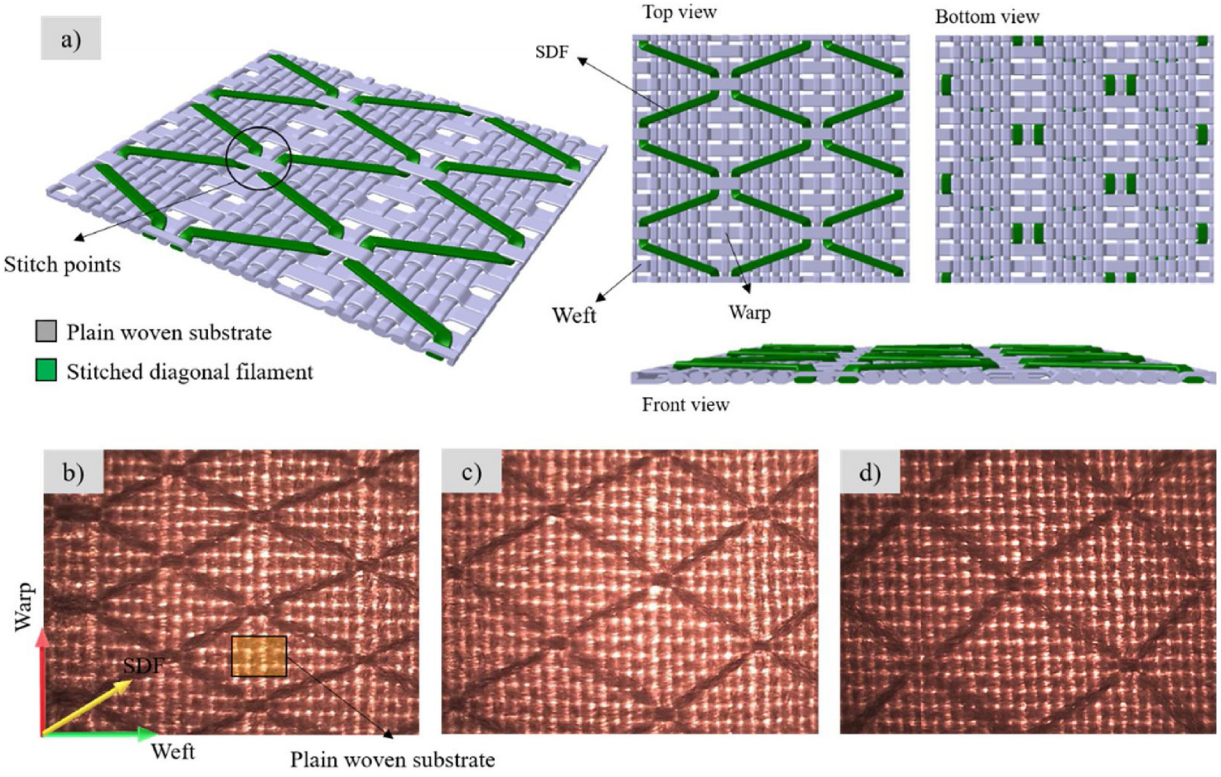


**Fig. 1.** a) Representative 3D schematic of a stitched plain-woven textile with 30° gradient of SDF and its constituents; b–d) Structural configuration of stitched plain reinforcements with gradients of 30°, 45° and 60°, respectively.

properties of these SPC obtained with mold temperatures of 140, 160, 180, and 200 °C were studied. The SPC obtained by reactive processing demonstrated a tensile strength of 154 MPa at molding temperature of 160 °C which was a 108 % increase as compared to the tensile strength of neat PA6 (74 MPa) at the same molding temperature. In a different study [12], the same authors investigated the effects of elevated mold temperature (222–228 °C) on the tensile properties of PA6-based SPC prepared by hot compaction of recycled PA6 cloth. In this study the processing window was about 5 °C.

Dencheva et al. [16] investigated the influence of the surface treatment of PA6 filaments on the tensile properties of PA6-based SPC prepared by in-mold AAROP of caprolactam. Three AAROP temperatures of 160, 165 and 170 °C were employed, being significantly lower than the melting point of the PA6 filaments (225 °C). The SPC obtained with 15–20 wt.% reinforcements and solvent pretreatment prior to AAROP showed a remarkable 70–80 % improvement of the stress at break and up to 150–190 % deformation at break compared to the neat PA6 matrix. The optimum AAROP temperature was 165 °C rendering a processing window of ca. 60 °C.

Tohidi et al. [21] studied textile reinforced SPC laminates produced by compression molding of PA6 knitted textile structures powder-coated with PA6 microparticles obtained by AAROP. The tensile properties of composites were assessed in relation to the knitted reinforcement architecture (Rib 1 × 1 and Jersey), fiber volume fraction $V_f$ of 15, 20 and 25 %, ply orientation (wale and course) and stacking orders (0/45/0 and 90/45/90). The processing window was about 8 °C that turned to be sufficient for avoiding undesirable reinforcement melting. Based on thickness discrepancies in the annealed monofilaments before and after their embedment in the SPC matrix, formation of a TCL at the fiber-matrix interface was supposed. Improvements of the tensile stiffness with 11 % and of the tensile strength of 18 % were registered, as compared to the anionic PA6 reference. The WAXS experiments performed displayed that the fracture behavior of the SPC depends on the crystalline morphology and $\alpha-\gamma$ PA6 polymorph content.

The flexural and impact properties of these SPC composites were considered in a subsequent study [22]. The anisotropic tensile and compression properties imparted by the knitted structures were found to be the major factors determining their mechanical properties. Microscopy studies provided proofs for the existence of TCL at the matrix-reinforcement interface being supported by the results of the deconvolution of the X-ray diffraction patterns of composites and neat textile reinforcements. The flexural and impact properties of SPC were considered as a function of the knitted reinforcement geometry and related to TCL.

In the present study, PA6-based single polymer laminate composites reinforced by conventional (plain and satin) and novel stitched plain-woven structures were produced and designated as WSPC. To produce the WSPC, all PA6 woven textile plies were powder-coated by PA6-based empty microcapsules (EMC) and consolidated by compression molding under optimized conditions. Powder impregnation technique was used for the preparation of all-polyamide laminate composites in this study to produce pulverulent polyamide-based materials. The EMC were synthesized previously via AAROP of ε-caprolactam (ECL) in suspension. The overall tensile and impact properties of WSPC were evaluated in relation to the reinforcement geometry, $V_f$ content and ply orientation. Differential scanning calorimetry (DSC), thermogravimetric analysis (TGA) and X-ray diffraction (XRD) were applied to elucidate the WSPC´s microstructure-mechanical properties relationship. Also, the interface morphology and structure of WSPC were studied applying image processing of scanning electron microscopy (SEM) micrographs and linked to the mechanical behavior. To the best of our knowledge, the novel class of stitched plain-woven structures has never been used before in SPC production. Therefore, a systematic comparative study with conventional plain-woven textiles for full morphological characterization of the WSPC on their basis is important for revealing the potential of these new SPC materials.

## 2. Materials and experimental test methods

### 2.1. Woven reinforcements

Conventional woven fabrics (plain, satin) and a novel stitched plain textile structure (SP) were selected as reinforcements. The SP textiles that contain plain structure substrates and stitched diagonal filaments (SDF) were fabricated in a NFM 6/42 loom at Jackob Müller AG®, Switzerland. The position of stitches controls the angle of SDF on stitched plain reinforcements (Fig. 1a). As it can be seen in Fig. 1b–d, three SDF gradients namely 30˚, 45˚ and 60˚ over the plain weave substrates were considered in this study for preparation of WSPC. Air jet textured PA6 continuous-filaments (160 dtex) were chosen to produce the fabric structure so as to rise the monofilaments entanglement and enhance the formation of the PA6 matrix material through the monofilaments during the WSPC preparation.

### 2.2. Pretreatment of the textile structures

To eliminate contaminations, all woven fabrics were pre-washed with the same type of non-ionic detergent solution at 30 ˚C for 30 min and then rinsed with reverse osmosis water for another 15 min. Next, they were immersed in acetone for 30 min and then dried for 120 min at 60 ˚C to remove any non-chemically bonded hydrophobic finish (oligomers) from the filament surface. Afterward, all reinforcements were stretched biaxially to 30 % of their original length using a specially designed metal frame and a screen stretching apparatus (Fig. 2a). The stretched reinforcements were then annealed with fixed ends at 170 ˚C for 90 min to enhance their crystallinity index and geometrical stability. Fig. 2c-d show the geometry changes of all woven reinforcements during the stretching-annealing procedure. Apparently, the latter causes the formation of voids in the textile reinforcements, which are expected to enhance their impregnation with matrix material during the WSPC consolidation by compression molding.

Table 1 shows the sample designation, the densities in warp and weft directions, the areal weights and thicknesses of the woven reinforcements before and after the stretching-annealing treatment.

### 2.3. Reagents

All the solvents used in this study are of puriss grade, purchased from Sigma Aldrich (USA). The ECL monomer was delivered by Brüggemann Chemical, (Germany). Prior to use, it was dried under vacuum for 1 h at 30 − 40 ˚C. The sodium dicaprolactamato-bis-(2-methoxyethoxo)-aluminate (DL) initiator was purchased from Katchem (Czech Republic). The activator C20 P (C20) was a product of Brüggemann Chemical, (Germany), containing 80 wt% of diisocyanate blocked in ECL. Both DL and C20 were used as received.

### 2.4. Synthesis of the PA6 microparticles

All laminate composites of this study were prepared by impregnation of PA6 textile structures with PA6 powder and subsequent consolidation by compression molding. While the textiles are made of a commercial hydrolytic PA6 with $T_m$ of 225 ˚C, the PA6 powder represents empty microcapsules (EMC) synthesized by activated anionic polymerization in solution with significantly lower $T_m$, which is attained by a stringent control over the polymerization process [18,21–23]. The term “empty microcapsules” is used to make a distinction from “loaded microcapsules” containing organic or inorganic payloads [18,23]. Generally, ECL is dissolved in toluene/xylene mixture, then the catalytic system (DL and C20) is added and the AAROP is carried out at 130 − 135 ˚C for 1 h. Then the reaction mixture is vacuum filtered, followed by washing of the residual EMC with methanol and vacuum drying. The chemical reaction of AAROP producing EMC is schematized in Fig. 3a.

The scanning electron microscopy (SEM) images in Fig. 3b display the typical morphology of the EMC microparticles used in thus study: spheroids with typical sizes in the 15 − 25 μm range and scaffold-like porosity observable at higher magnifications.

### 2.5. Preparation of WSPC

The WSPC were produced using powder-coating (PC) of the textile structures with EMC and subsequent consolidation by compression molding (CM), this method being designates as PCCM. A Moore hydraulic hot press (UK) equipped with a mold with dimensions 70 × 70 × 2 mm were employed to consolidate the WSPC. The mold pressure and temperature were set at 5 MPa and 215 ˚C, respectively (Fig. 4). Afterward, the samples were cooled down to 50 ˚C at a rate of ca. 40 $°C/min$. Various reinforcement architectures, fiber contents and ply orientation were employed in this study (Table 2). Thus, three fiber volume fractions $V_f$ of 15, 20 and 25 % were selected to prepare WSPC. Higher $V_f$ values caused rupture of the embedded woven reinforcements under the selected conditions of consolidation. The number of textile plies for each $V_f$ was determined according to the following equation [24]:

$$N = \frac{V_f . \rho_f . t}{A_w} \quad (1)$$

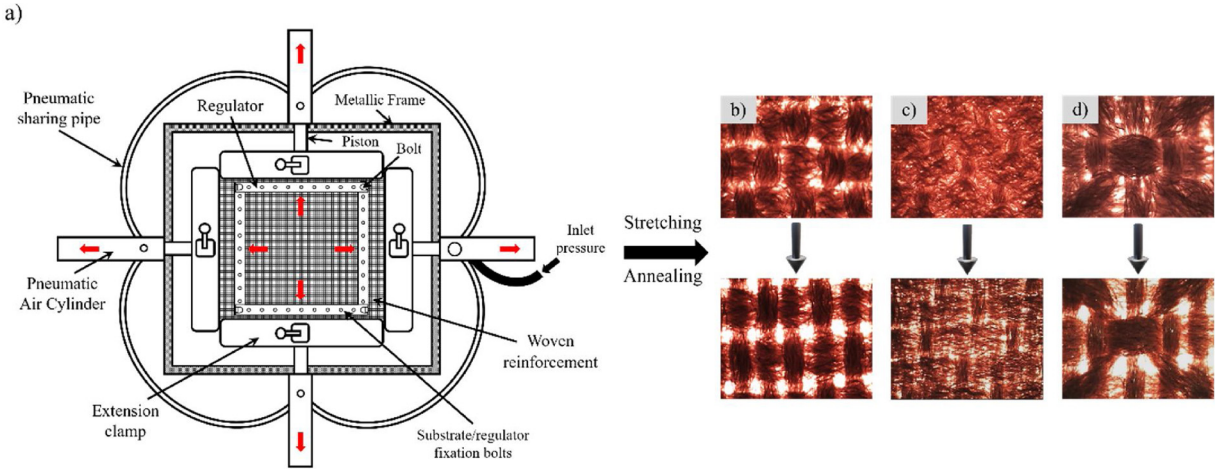


**Fig. 2.** a) Schematic of a biaxial stretching screen stretcher apparatus; Stretching-annealing treatment of the textile structures and structural deformation (from top to the bottom) of b) Plain; c) Satin (5-harness); d) SP45 (as representative sample).

**Table 1**
Sample designation and properties of the woven reinforcements.

| Reinforcement type | Treatment | SDF gradient | Sample Designation | Warps/cm | Wefts/cm | Areal weight (g/m$^2$) | Thickness (mm) |
|---|---|---|---|---|---|---|---|
| Plain | No | – | P | 22 | 16 | 147.6 ± 1.7 | 0.58 ± 0.01 |
| | YES | – | P-A | 20 | 12 | 111.0 ± 1.1 | 0.42 ± 0.01 |
| Satin | No | – | S | 22 | 16 | 142.4 ± 1.3 | 1.00 ± 0.02 |
| | YES | – | S-A | 22 | 12 | 106.5 ± 1.6 | 0.46 ± 0.01 |
| Stitched Plain | No | 30 | SP30 | 22 | 14 | 138.4 ± 0.9 | 0.61 ± 0.01 |
| | No | 45 | SP45 | 22 | 14 | 128.1 ± 1.1 | 0.55 ± 0.01 |
| | No | 60 | SP60 | 22 | 14 | 131.3 ± 1.0 | 0.55 ± 0.01 |
| | YES | 30 | SP30-A | 19 | 12 | 111.8 ± 1.0 | 0.41 ± 0.01 |
| | YES | 45 | SP45-A | 19 | 12 | 108.7 ± 1.6 | 0.37 ± 0.01 |
| | YES | 60 | SP60-A | 19 | 12 | 110.4 ± 2.1 | 0.38 ± 0.01 |

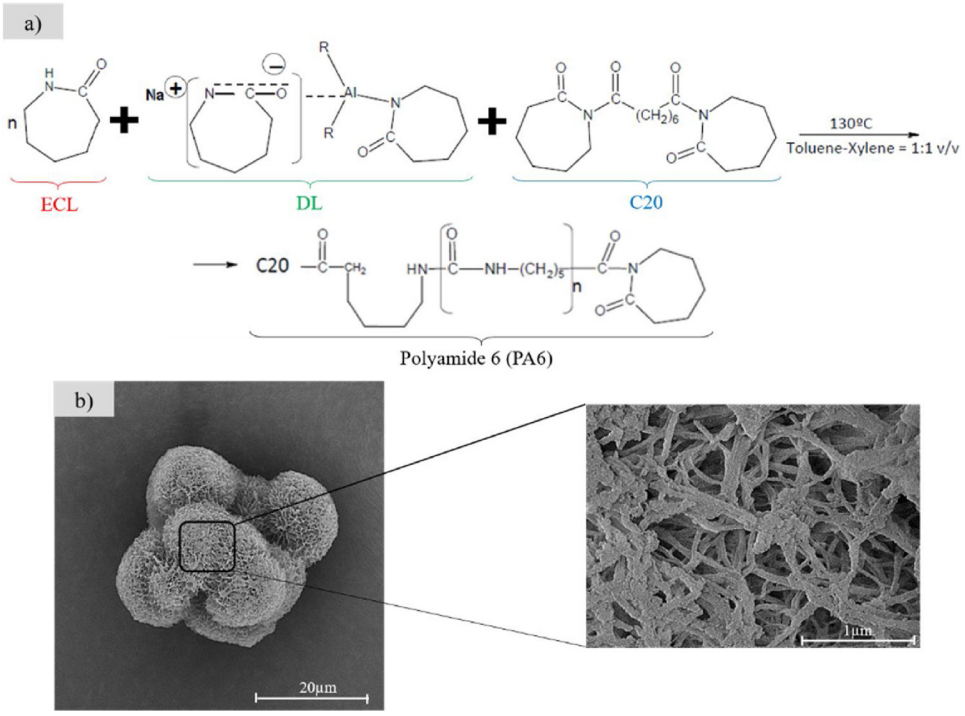


**Fig. 3.** a) Chemical reactions occurring during AAROP in solution: C20 Bruggolen C20 (activator), DL dicaprolactamato-bis-(2-methoxyethoxo)-aluminate, $R = OCH_2CH_2OCH_3$ [23]; b) Selected SEM micrographs of PA6 empty microcapsules and magnified images (inset image).

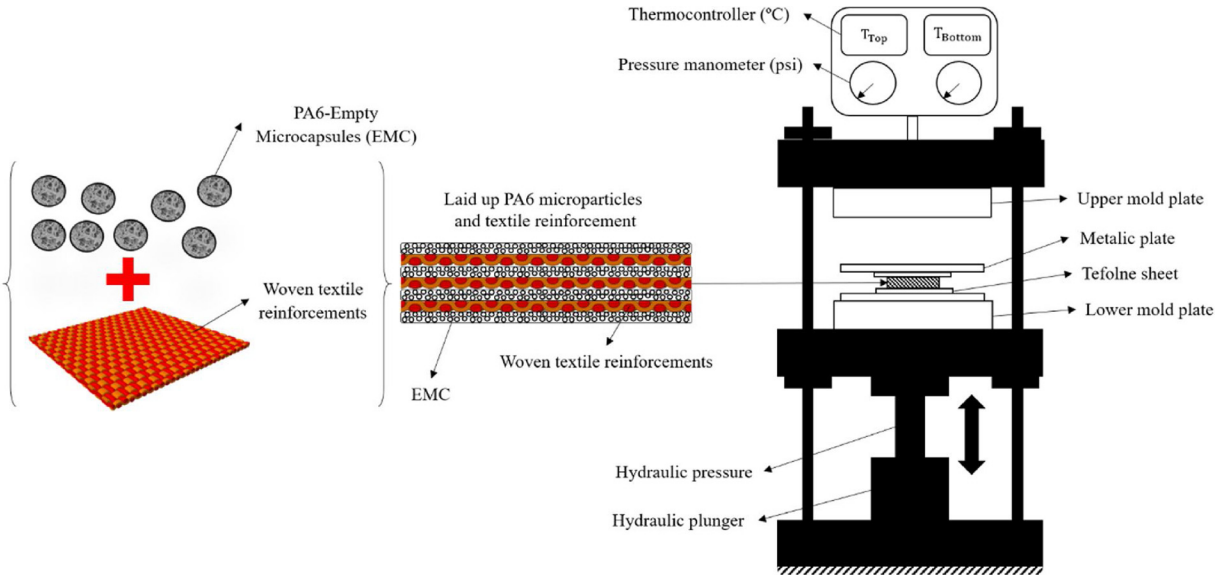


**Fig. 4.** Schematic of laying up and compression molding of laid up PA6 microparticles matrix and woven textile reinforcements constituents (PCCM technique).

**Table 2**
Description and designation of the WSPC laminate composites prepared.

| WSPC designation | | | $V_f$,% | Plies Number |
|---|---|---|---|---|
| Plain reinforced WSPC | *P-WSPC* | *P [a] (0 [b])-15* | 15 | 3 |
| | | *P (90)-15* | 15 | 3 |
| | | *P(0)-20* | 20 | 4 |
| | | *P(90)-20* | 20 | 4 |
| | | *P(0)-25* | 25 | 5 |
| | | *P(90)-25* | 25 | 5 |
| Satin reinforced WSPC | *S-WSPC* | *S [c] (0)-15* | 15 | 3 |
| | | *S [c] (90)-15* | 15 | 3 |
| | | *S(0)-20* | 20 | 4 |
| | | *S(90)-20* | 20 | 4 |
| | | *S(0)-25* | 25 | 5 |
| | | *S(90)-25* | 25 | 5 |
| Stitched Plain reinfoced WSPC | *SP-WSPC* | *SP[d]30 [e]-(0)-15* | 15 | 3 |
| | | *SP45 -(0)-15* | 15 | 3 |
| | | *SP60 -(0)-15* | 15 | 3 |
| | | *SP30-(90)-25* | 25 | 5 |
| | | *SP45-(90)-25* | 25 | 5 |
| | | *SP60-(90)-25* | 25 | 5 |

[a] P stands for Plain reinforcements.
[b] Unidirectional lamination in which 0° or 90° stand for warp-wise and weft-wise directions respectively.
[c] S stands for Satin reinforcements.
[d] SP represents Stitched Plain reinforcements.
[e] The SDF angles are presented as 30°, 45° and 60°. For better perception see Fig.1 and Table 1.

Where $\boldsymbol{N}$ is the number of plies, $\boldsymbol{\rho_f}$, (g.m$^{-3}$) is the density of the PA6, $\boldsymbol{A_w}$, (g.m$^{-2}$) is the area density of the textile reinforcement, and **t** (m) is the laminate thickness [24]. To produce a laminate WSPC with k plies, the respective EMC amount was divided into (k + 1) equal portions and the respective ply sets were prepared and compression molded as schematized in Fig. 4.

Apart from the $V_f$ values, Table 2 shows also all details about the ply types and their orientations, as well as all sample designations.

### 2.6. Morphological characterization

To evaluate the morphology in the matrix/reinforcement interface region, SEM studies were performed in a NanoSEM-200 apparatus of FEI Nova (USA) using mixed secondary electron/back-scattered electron in-lens detection. Au/Pd alloy was employed to sputter-coat the samples to be observed. For dimensional image analysis of original monofilaments in treated woven reinforcements, an Olympus BH-2 light microscope (Japan) equipped with Leica Application Suite 4 software was used. The micrographs of the monofilaments before and after embedment were treated according to an algorithm written in Python with the use of Open CV library.

Ubbelohde viscometer thermostatted at 25 °C was used to measure the average viscometric molecular weight $M_v$ of the as-prepared EMC and woven reinforcements. The intrinsic viscosity measurements in 97 % sulfuric acid at a concentration of 0.2 $g/dL$ was considered in which the Mark-Houwink equation for PA6 was applied with K= 5.066. $10^{-4}$ and $\alpha = 0.74$ [25]. The woven textile reinforcements contained average viscometric molecular weight $M_v$ of ca. 39,500 g/mol which was slightly higher than $M_v$ of the as-prepared EMC (36,500 g/mol).

The thermal properties of WSPC and precursors were investigated using differential scanning calorimetry (DSC) studies in a 200 F3 equipment of Netzsch (Germany) at a heating rate of 10 °C.min$^{-1}$ under nitrogen purge. The typical weights of the samples were in the 6 − 16 mg range. The glass transition temperature, the processing window and the degree of crystallinity were extracted from each DSC curve. Two consecutive heating scans were performed. In between, crystallization at a cooling rate of 10 °C/min was applied. The crystallinity index $X_C^{DSC}(\%)$ of the samples was calculated according to Eq. 2:

$$X_C^{DSC}(\%) = \frac{\Delta H_m^i}{\Delta H_m^\circ} \quad (2)$$

wherein $\Delta H_m^i$ is the registered melting enthalpy of the current sample and $\Delta H_m^\circ$ is the melting enthalpy of a 100 % crystalline PA6 (230 J/g) [26].

Thermogravimetric analysis was performed in a modulated TGA Q500 from TA instruments. The TGA trace was obtained in the range 40–600 °C under the nitrogen atmosphere with a flow rate of 20 mL.min$^{-1}$, the heating rate being 10° C.min$^{-1}$. The samples were dried at 60 °C for 1 h before test performance. TGA curve, its first derivative, as well as the DTA curve were obtained and analyzed for all samples.

The wide-angle X-ray scattering (WAXS) patterns of the textile reinforcements, EMC, neat matrices and WSPC laminates were collected in a Bruker D8 Discover θ-θ diffractometer working with Cu Kα radiation (λ = 1.541 Å) and in the 2θ range of 5-45° at a rate of 0.1 deg.min$^{-1}$. A commercial peak-fitting software was used to curve fitting of the WAXS patterns as previously described [27]. The WAXS crystallinity index $X_c^{WAXS}$, was calculated according to Eq. 3:

$$X_c^{WAXS}(\%) = \frac{\sum A_c}{\sum A_c + \sum A_a} \quad (3)$$

where $\sum A_c$ is the integrated area under the respective crystalline peaks and $\sum A_a$ is the integrated area of the amorphous halo(s). The D-spacing which is the spacing (Å) between planes in an atomic lattice of matrix and reinforcements precursors were calculated from Bragg's law.

### 2.7. Mechanical characterization

ASTM D5034 (grab test) was applied for tensile evaluation of woven reinforcements with 150 × 100 mm dimension using Instron 4505 machine with a standard load cell of 2.5 kN and at a constant crosshead speed of 2 mm.min$^{-1}$. The tensile test of the treated woven textiles was performed in the same day of its stretching and annealing with fixed ends (see section 2.2). After their preparation, the laminate WSPC were stored for 30 days at 23 °C and 65 % relative humidity, i.e., subjected to conditioning. The tensile test was performed in the same testing machine at 23 ± 2 °C with a standard load cell of 50 kN and at a constant crosshead speed of 2 mm.min$^{-1}$. The tensile tests were carried out according to ASTM D638. For every WSPC at least 5 test specimens with gauge length of 38 mm were tested being laser cut from the same laminate plate.

Izod impact pendulum tester was used to measure impact strength of the unnotched WSPC according to ASTM D256-04 standard with 22 mm height at the strike point. The impact strength (I) was determined by the impact energy absorbed by the sample cross-section, according to equation:

$$I\left(\frac{KJ}{m^2}\right) = \frac{E_{WSPC} - E_o}{A} \quad (4)$$

where $E_o$ and $E_{WSPC}$ are the impact energies registered without and with the sample, respectively, and A is the area of the sample.

## 3. Results

### 3.1. Matrix/reinforcement bonding state

In composite materials, evaluation of bonding state at the fiber-matrix interface is essential for understanding of their mechanical performance. The preparation of the WSPC by the PCCM technique includes a stage wherein the molten matrix-forming PA6 material originating from EMP crystallizes epitaxially upon oriented crystalline PA6 filaments. Therefore, there exist all conditions for the formation of

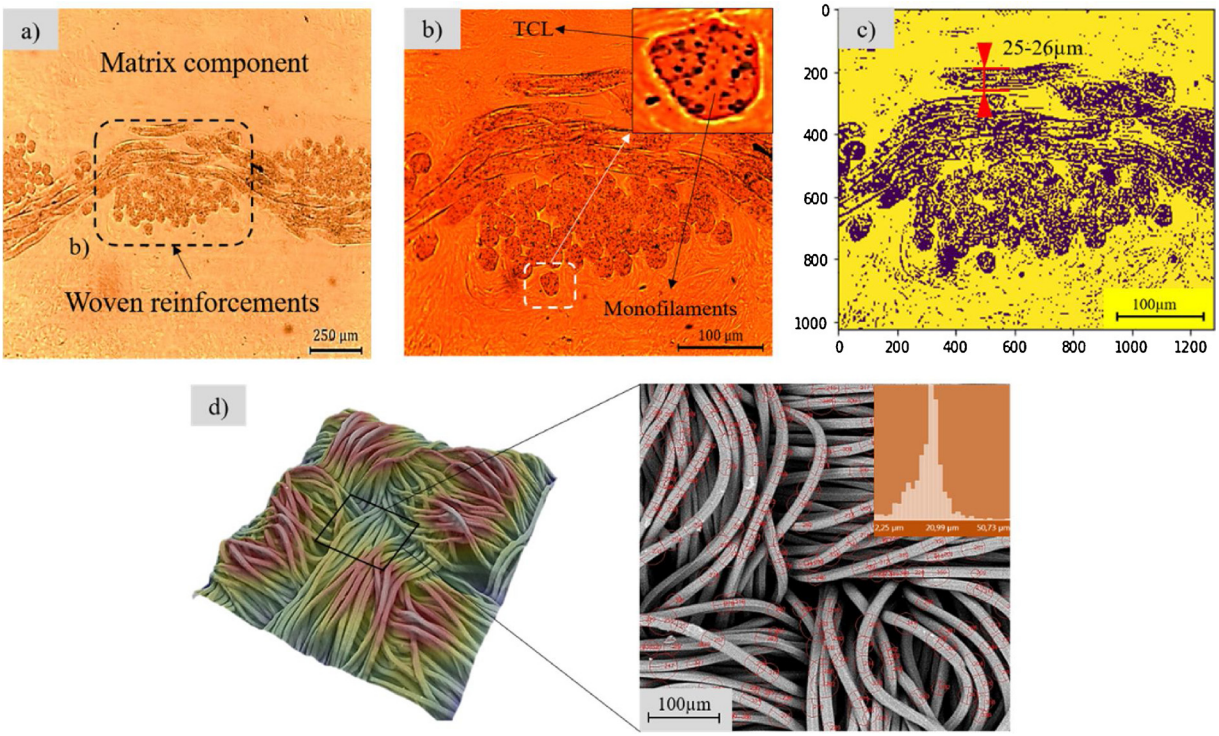


**Fig. 5.** a) Microscopic image of P(0)-15 sample with visible light; b) Detection of TCL at matrix-reinforcement interface region; c) Thickness measurement of embedded monofilaments in microscopic surface topography of P(0)-15 sample; d) SEM microscopic image of treated plain-woven reinforcement with application of image thresholding, erosion and dilation for noise elimination. The magnified area depicts the average thickness measurement of the monofilaments in the P-A textile structure before its inclusion in a WSPC.

transcrystalline layers (TCL) upon the filament surface [28,29]. More particularly, TCL was established and thoroughly studied in polymer-polymer in-situ composites [30–32]. More recent study on finite element mesoscale modeling of PA6-based single polymer laminate composites clearly displayed the need to consider the TCL as an important factor influencing their mechanical properties [33]. To characterize the matrix-fiber interface state in the WSPC prepared, microstructural studies were carried out by means of polarized light microscopy (PLM) and SEM.

Fig. 5a demonstrates a PLM image of the P(0)-15 sample. The isotropic matrix and the oriented fiber reinforcements are depicted in bright (yellowish) and darker (brown) colors, respectively. A thin bright halo at the boundaries between the matrix constituent and the monofilament embedded in it are detected in Fig. 5b. This is an evidence for a distinct birefringent morphology attributed to the formation of TCL.

To prove quantitatively the TCL presence, the thickness of the monofilaments in the fibrous reinforcement before and after embedment in a WSPC are compared. Thus, the average thickness of embedded monofilaments in P(0)-15 as evidenced by Fig. 5c is 25.0 ± 0.2 µm. The microscopic image of stretched and annealed plain reinforcement is shown in Fig. 5d after averaging and digital removal of noises showing that the average diameter of the original monofilament prior to its inclusion in WSPC is 23.0 ± 0.1 µm. Therefore, the average thickness of TCL should be close to 2 µm.

The representative SEM images of cryogenically fractured WSPC reinforced by 15 v.% P-A, S-A and SP30-A structures is visualized in Fig.6 a–f. No cracks, voids or other morphological defects at the fiber-matrix interface were observed (Fig. 6a). Apparently, the reinforcing filaments fail mechanically without a significant delamination from the matrix (Fig. 6b-c), whereby non-circular configuration in the region of break is formed (Fig. 6e). This observation is in favor of a good adhesion at the matrix-fiber interface. Fig.6c confirms an average thickness of the textile monofilament embedded in the WSPC of 25 − 26 µm. Some embedded reinforcing filaments being partially detached from the matrix (Fig.6b, 6d and 6f) evidence the TCL coating upon them with an orientation that is distinct from that of the monofilament interior part [33].

### 3.2. Differential scanning calorimetry

DSC was used to investigate the thermal behavior of the WSPC. Key parameters such as the width of the processing window, glass temperature transition and degree of crystallinity of the WSPC and their precursors were extracted from the DSC traces. Fig. 7a demonstrates the first heating scan of all types of woven reinforcements and the EMC. The processing window was calculated as the difference between the peak melting temperature of EMC and the peak melting temperature of the woven textiles. This difference is of 16 − 17 °C which was sufficient to produce WSPC with no risk of monofilaments melting during the consolidation. The lower melting temperature of the anionic EMC precursor ($T_{m-EMC}$ ≈207 °C) as compared to that of the textile reinforcements ($T_{m-R}$ ≈224 °C) could be explained with the lower $M_v$ of the former and of its micro-sized isotropic morphology. The broad low-temperature endothermic peaks centered at 85 °C in the starting woven reinforcements (Fig. 7a, curve 1) remain unaffected after the stretching-annealing treatment (Fig. 7a, curve 2). These peaks are attributable to a relaxation processes within the woven reinforcements taking place slightly above the glass transition temperature. It vanishes completely during the second DSC scan (Fig. 7b). The broad low-temperature endothermic peak during the first DSC scan of EMC centered at 100 °C was attributed to evaporation of moisture that the porous micron-sized EMC particles absorbed prior to the DSC scan.

The maximums of the endotherms in Fig. 7a should be related to the melting of the α polymorph of PA6 ($T_{m-\alpha}$ ≈223 °C). Fig. 7b shows the second DSC scan of all WSPC precursors wherein the $T_g$ of all samples was clearly detectable after eliminating the samples´ thermal history. Notably, the $T_g$ of EMC is lower than that of the textile structures thus revealing a higher segmental mobility of the polymer chains in the

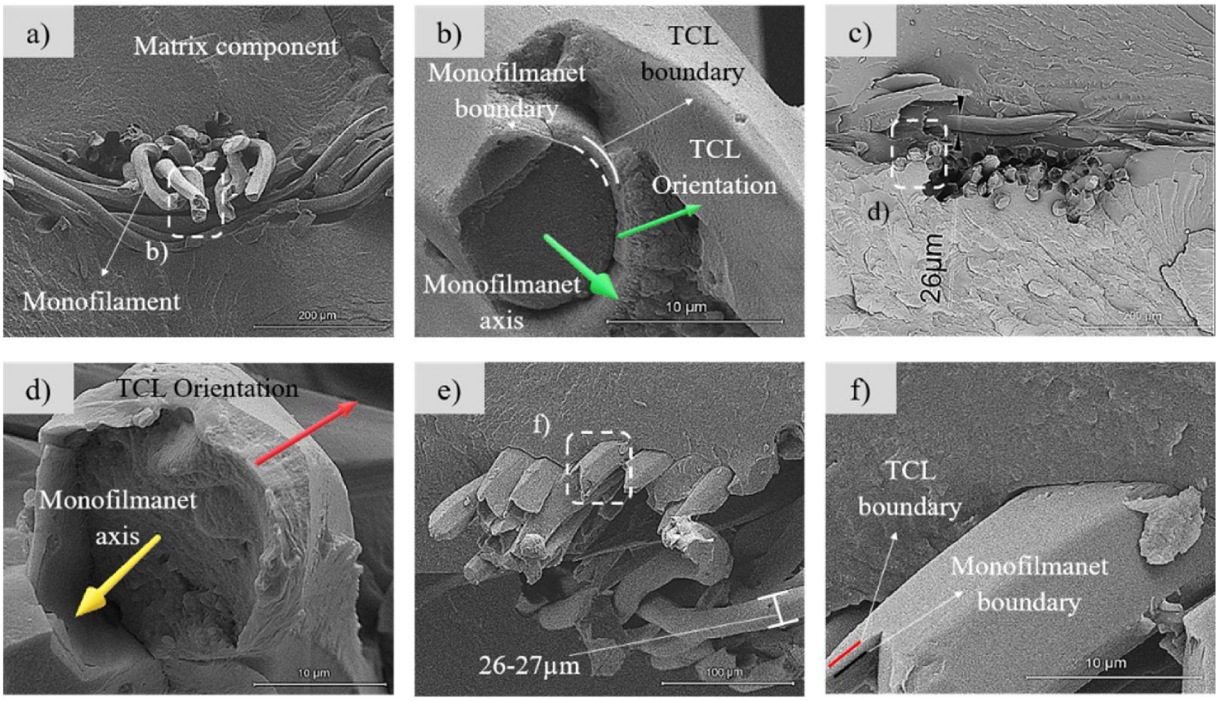


**Fig. 6.** SEM surface topography with 15 % fiber volume fraction of WSPC reinforced by a–b) P-A c–d) S-A e–f) SP30-A. For sample designation see Table 1.

anionic PA6 powder. Melting of some amount of anionic γ-PA6 polymorph was revealed as weak shoulders below 215 °C in all samples in Fig. 7b.

The first and second DSC scans of unidirectional WSPC (curves 2–4) compared to that of an anionic PA6 plate produced by compression molding of EMC (curve 1) are shown in Fig. 8a and 8b, respectively. The first scan DSC curve of PN displayed a single melting peak ($T_{m-PN}$ = 210 °C), whereas a bimodal melting endotherm was registered for WSPC with $T_{m1}$ = 208 − 210 °C and $T_{m2}$ = 214 − 219 °C (Fig. 8a). The former can be related with melting of PA6 originating from the matrix constituent and the later - to the fusion of the hydrolytic PA6 woven reinforcements. The second DSC scans of PN and WSPC samples show a weak shoulder at ca 200 °C related to the existence of γ -PA6 phase resulting after the WSPC fusion, along with the nominal melting peat at ca. 215 °C for the α-PA6 (Fig. 8b). The corresponding quantitative DSC data of all WSPC and their precursors extracted from the DSC traces are shown in Table 3.

As it can be seen from Table 3, all WSPC demonstrated bimodal melting peaks irrespective of their composition. As expected, the first melting point $T_{m1}$ roughly corresponds to that of EMC or PN, and the second $T_{m2}$ in the 214 − 218 °C is with up to 10 °C below the melting of the textile reinforcements. These low $T_{m2}$ values could be attributed to interchange reactions between PA6 from the matrix and from the reinforcements taking place during the WSPC consolidation or the proper DSC experiment. These interchange reactions can lead to the formation of chemical bonds across the anionic matrix and hydrolytic filament interface thus enhancing the adhesion [34]. The DSC crystallinity $X_c^{DSC}$ of the initial plain-woven textile structure P grew slightly after stretching-annealing to P−A, whereas in the altering reinforcements this treatment did not change significantly $X_c^{DSC}$. Fiber volume fraction and reinforcement architecture had no significant changes on glass transition temperature and the degree of crystallinity in WSPC. It should be mentioned that embedding the woven reinforcements in an anionic PA6 matrix originating from the EMC lowered the $T_g$ and $X_c^{DSC}$ of WSPC to the same level as in PN. The lower $X_c^{DSC}$ value of PN as compared to EMC could be a result from the faster cooling rate during the compression molding.

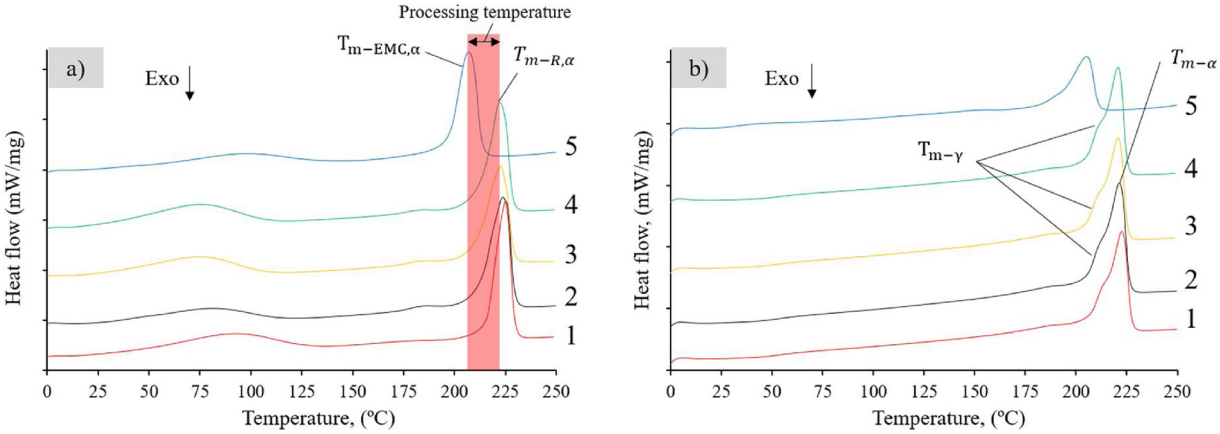


**Fig. 7.** DSC thermograms of WSPC building constituents: (a) 1 st DSC scan; (b) 2nd DSC scan. 1- P; 2- P-A; 3- S-A; 4- SP30-A; 5- Anionic EMC. For sample designation see Table 1.

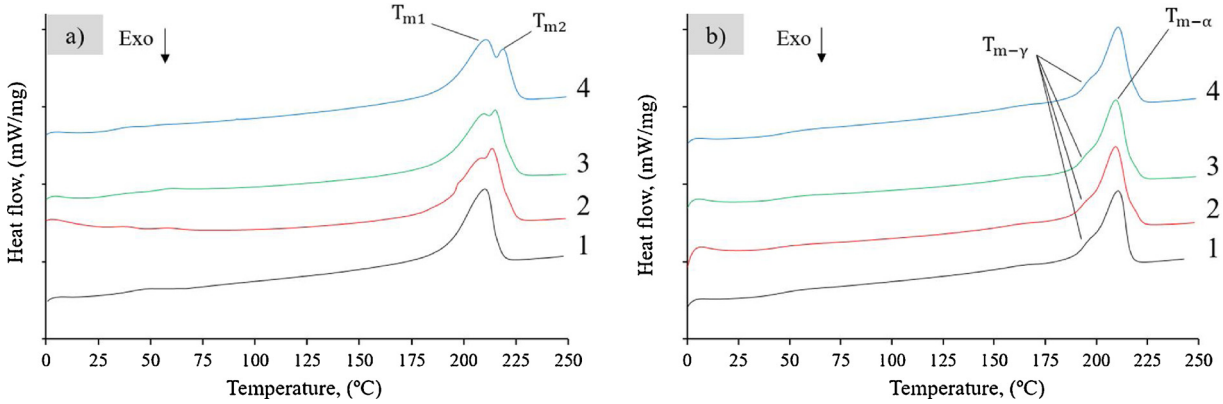


**Fig. 8.** DSC curves of WSPC from hot compacted EMC-impregnated woven textile structures: (a) 1 st DSC scan; (b) 2nd DSC scan.: 1 – PN; 2 –P(0)-15; 3 –S(0)-15; 4 –SP30(0)-15. For sample designation see Table 2.

**Table 3**
Crystallinity index for WSPC and their precursors. For sample designation see Tables 1 and 2.

| Sample designation | $T_g$ (°C) | $T_{m1}$ (°C) | $T_{m2}$ (°C) | $X_c^{DSC}$, % |
|---|---|---|---|---|
| EMC | 32.3* | 207.8 | – | 34.9 |
| PN | 33.3 | 210 | – | 27.5 |
| P | 50.7* | – | 224.9 | 37.2 |
| P-A | 48.1* | – | 223.5 | 41.8 |
| S-A | 48.9* | – | 222.5 | 38.3 |
| SP30-A | 52.4* | – | 222.2 | 39.2 |
| SP45-A | 51.8* | – | 224.8 | 35.7 |
| SP60-A | 50.9* | – | 222.2 | 37.3 |
| P(0)-15 | 32.9 | 208.7 | 213.6 | 33.0 |
| P(0)-20 | 30.8 | 209.5 | 215.8 | 31.9 |
| P(0)-25 | 30.3 | 209.8 | 217.3 | 31.0 |
| S(0)-15 | 31 | 209.6 | 215 | 32.5 |
| S(0)-20 | 30.8 | 209.4 | 217.2 | 30.6 |
| S(0)-25 | 33.1 | 209.4 | 218.6 | 32.2 |
| SP30(0)-15 | 34.1 | 210.5 | 219.2 | 30.9 |
| SP45(0)-15 | 30.8 | 209.7 | 215.7 | 34.0 |
| SP60(0)-15 | 33.5 | 210.7 | 217.7 | 33.4 |
| SP30(0)-25 | 33 | 209.9 | 217 | 30.9 |
| SP45(0)-25 | 33.7 | 211.1 | 217.8 | 33.8 |
| SP60(0)-25 | 32.4 | 210.4 | 217.6 | 29.6 |

*$T_g$ determined during the 2nd DSC scan.

### 3.3. Thermogravimetry with simultaneous differential thermal analysis

The WSPC and their precursors were further subjected to thermogravimetry (TGA) combined with differential thermal analysis (DTA). Thermal characterization of composites and precursors were performed to determine the threshold temperatures in the WSPC consolidation by compression molding. This was important since the processing window in SPC materials is quite narrow and any overshooting above the $T_m$ of the textile structure will deteriorate the mechanical properties. Moreover, thermogravimetric analysis in this study provides beneficial information about the end-use applications of WSPC materials. Fig. 9a shows the TGA/DTA curves of P-A reinforcement as representative sample in which three different plots as a function of the temperature, namely the weight loss (TGA, %), enthalpy/entropy changes (DTA, μV) and derivative thermal gravimetry (DTG, μg/min) were included. The data extracted from the TGA curves are displayed in Table 4. The initial decomposition temperature (IDT) illustrates the onset of the weight losses, $T_m$ is the melting temperature and MRD/MRDT the temperature of maximum degradation rate. The latter is considered as the inflection point of the integral TGA. As it can be seen in the Fig. 9a, the P-A sample displayed a $T_m$ at 213 °C in the DTA trace and a multiple endotherm of thermal degradation centered around 440 °C. The DTA traces of PN, i.e., the neat matrix from EMC showed a single $T_m$ peak at 200 °C and a well-expressed single thermal decomposition isotherm at 330 °C (Fig. 9b).

The thermogravimetric traces of WSPC and precursors are shown in Fig. 9c. As expected, all WSPC (curves 3–7) demonstrated higher thermal stability than the EMC matrix constituent (curve 1) but lower than that of the plain textile reinforcement P and P-A (curves 3,4). As seen from Fig. 9c, all composites in this study decomposed thermally in a similar way at MRDT visibly below 350 °C, whereas the textile reinforcements are considerably more thermally stable with MRDT values close to 450 °C. Generally, the major weight loss of WSPC samples took place in the range of 340 − 350 °C. Increasing the fiber volume fraction delayed the degradation rate observably.

### 3.4. X-ray diffraction studies

The SPC concept requires reinforcing a PA6 matrix with PA6 textile structures is not a straightforward objective. In trying to do that one needs to manipulate the microstructure of the matrix and of the textile in such a way so as to secure (i) the necessary processing window and (ii) the optimal difference in the mechanical properties of the matrix and textile PA6. All this is impossible without a rigorous study of the melting-recrystallization behavior of the two constituents, which brings us to the crystalline structure and polymorphism. There is beyond any doubt that the mechanical properties of PA6 depend on the its polymorph composition, the α-PA6 being more rigid and the γ-PA6 being more ductile [35]. It is the thermal regime during the consolidation process (maximal temperature, time duration of compression molding, rate of cooling down etc.) that will form the respective crystalline structures. That is why in this study, along with the TGA and DSC, XRD was implemented to study the crystalline structure of WSPC and their precursors. Peak fitting was performed by deconvolution of the linear diffraction patterns of all samples attaining fitting coefficients $r^2 \approx 0.99$. Representative X-ray patterns of plain reinforcements before and after heat-stretching, and the respective deconvolutions are shown in Fig. 10a-b respectively.

As found in previous studies with PA6 samples [36,37], the two peaks with 2θ at ca. 20° and 23° correspond to the [200] and [002/202] crystalline planes of an α -phase monoclinic unit cell. The two Gaussian peaks at 2θ between 21 and 22° correspond to γ[001] and γ[200] crystalline planes and characterize the pseudo-hexagonal unit cell of the γ-PA6 polymorph. Two wide Gaussian peaks ($AM_1$ and $AM_2$) were used for the diffuse scattering of the amorphous PA6 fraction. The XRD pattern of untreated plain structure P shows slightly asymmetric α-crystalline reflections (Fig. 10a) that, upon stretching and annealing in the P−A sample become with almost equal intensities and widths, being at the same time significantly stronger than the γ[001] and γ[200] crystalline reflections (Fig. 10b). The fitted XRD patterns of P−A, S-A− and SP30-A reinforced WSPC are represented in Fig. 11 b–d, compared

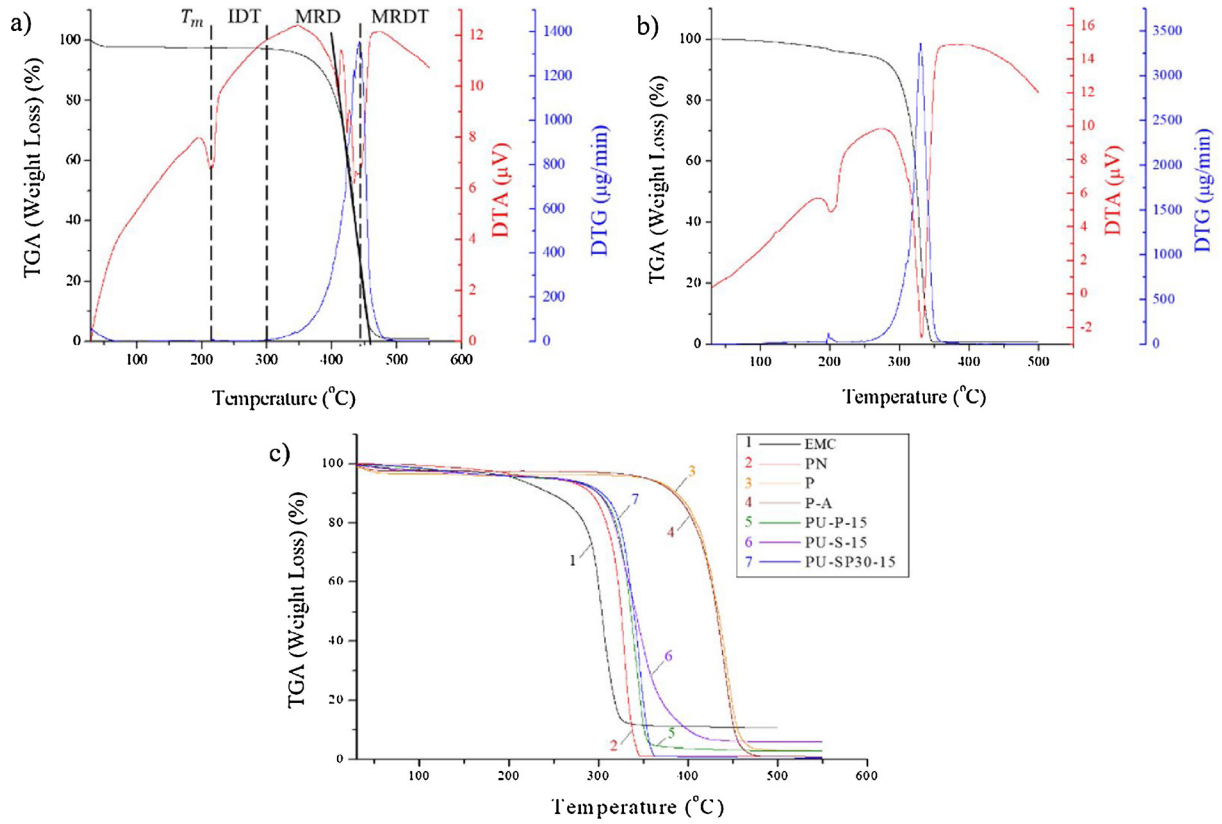


**Fig. 9.** DTA analysis in nitrogen atmosphere at 10 °C.min$^{-1}$ heating rate of: a) P-A; b) PN; c) TGA curves of WSPC and the precursors. For sample designation see Tables 1 and 2.

**Table 4**
TGA data analysis for WSPC and their precursors. For sample designation see Tables 1 and 2.

| Sample | $T_m$ (°C) | IDT (°C) | MRDT (°C) | MRD (Rad) | Degradation (%) |
|---|---|---|---|---|---|
| P | 217 | 311 | 444 | 1.09 | 92.4 |
| P-A | 215 | 302 | 441 | 1.12 | 95.4 |
| PN | 200 | 200 | 330 | 1.30 | 98.0 |
| EMC | 204 | 204 | 307 | 1.18 | 85.0 |
| P(0)-15 | 204 | 252 | 346 | 1.20 | 92.7 |
| P(0)-20 | 202 | 226 | 332 | 1.11 | 99.2 |
| P(0)-25 | 201 | 224 | 351 | 0.74 | 97.1 |
| S(0)-15 | 203 | 234 | 343 | 0.92 | 89.0 |
| SP30(0)-15 | 204 | 243 | 347 | 1.20 | 97.7 |
| SP45(0)-15 | 203 | 216 | 338 | 1.06 | 89.4 |
| SP60(0)-15 | 203 | 229 | 349 | 1.00 | 98.4 |

to that of anionic PA6 obtained from EMC and designated as PN (Fig. 11a).

In all WASPC patterns, a clear distinction between the α[200] and α[002/202] reflections of the anionic PA6 matrix and of the hydrolytic PA6 reinforcements was achieved. The broader and less intense peaks of the α-polymorph in the three representative WSPC samples correspond to the smaller and isotropic PA6 matrix crystallites formed after melting and recrystallization of the anionic EMC during the WSPC preparation. The more intense α-PA6 peaks are attributable to the stretched and annealed PA6 filaments of the textile plies that are embedded without melting into the matrix during the WSPC preparation. Thus, in all WSPC materials the matrix and the reinforcement constituents contain α-PA6 polymorphs with similar but distinguishable unit cell parameters, whose content can be quantified accurately as a function of the reinforcement architecture.

The γ-phase in the WSPC was fitted with four Gaussian peaks, being impossible to resolve if they belong to the matrix or to the reinforcement material. This, however, permits evaluation of the total amount of α- and γ-PA6 polymorphs in all WSPC as a function of the reinforcement type. The consolidated information extracted from the XRD patterns deconvolution of all WSPC and their precursors (EMC, PN, textile structures before and after annealing) is presented in Table 5, including data about the contents of γ- and α-PA6 polymorphs, their relation $\frac{\alpha}{\gamma}$, the total crystallinity index $X_c^{XRD}$, and the respective long spacing of the peaks.

The data in Table 5 show that the total $X_c^{XRD}$ of the WSPC with plain woven and satin reinforcements (P- and S- samples) is with 5–10 % higher than in the WSPC with stitched reinforcements (SP samples). The total $\frac{\alpha}{\gamma}$ polymorph ratio is in average close to 2, extreme values of 2.37 and 1.56 being registered with the P(0)-25 and SP30(0)-15 composites, respectively. Thus, provided that the consolidation conditions for all WSPC were strictly the same, it seems that the architecture of the reinforcing textiles may influence the total crystallinity and, to a lesser extent, the polymorph ratio. The structural data in Table 5 show also that in all WSPC samples the content of the α-PA6 found in the textile reinforcements is always higher than that located in the PA6 matrix. Judging from the structural data of the WSPC precursors, melting the EMC to PN (i.e., the production pure matrix material at the conditions of WSPC consolidation) results in PA6 with relatively low crystallinity index of 35 % with $\frac{\alpha}{\gamma} = 1$. Stretching and annealing of the textile precursors (e.g., P and P−A samples) led to a moderate increase of $X_c^{XRD}$ values with 4 %. The content of α-PA6 in the annealed textiles, however, increases more than two times, i.e., from $\frac{\alpha}{\gamma} = 1.7$ to 4. Therefore, the polymorph ratio in the WSPC of ca. 2.0 is explained with the combination of the $\frac{\alpha}{\gamma}$ values in the matrix and the textile reinforcements. In such a way, the embedded textile reinforcements whose $V_f$ is among 15–25 % influence the crystalline structure of the WSPC, in which the isotropic anionic PA6 originating from EMC is the major constituent.

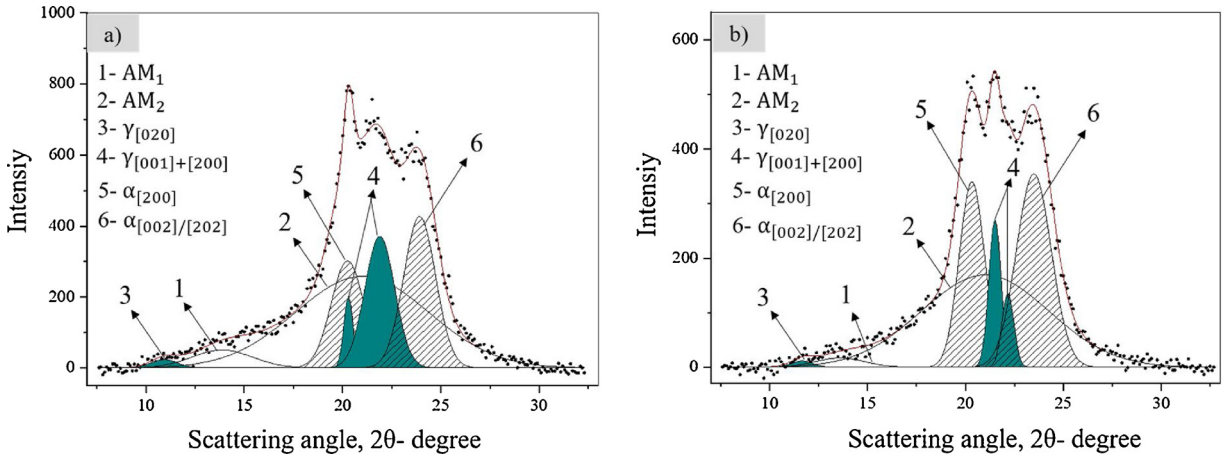


**Fig. 10.** WAXS patterns and their fits of WSPC precursors: a) untreated plain reinforcement (P); b) stretched-annealed plain reinforcement (P−A). $AM_1$ and $AM_2$ = diffuse peaks of the amorphous PA6.

Table 5 presents also the D-spacings of all PA6 peaks identified in the WSPC and their precursors. The values suffer very small changes with the $V_f$ and architecture of the textile reinforcement are identical to those of oriented and isotropic PA6 found in the literature [16]. Since the mechanical properties of PA6 are closely related to the crystallinity index and polymorph content [16,21], the structural obtained by XRD will be correlated with the mechanical data.

### 3.5. Mechanical behavior in tension

The mechanical studies started by testing in tension all woven reinforcements, before and after the stretching-annealing treatment. As seen from the stress-strain curves in Fig. 12a exemplifying two types of stitched plain reinforcements, the treated samples (SP60(0)-A and SP60(90)-A) showed a clear elastic region in the stress–strain curves starting between 2–5 % of strain, whereas in the initial textiles the said elastic regions start above 10–15 % deformation. This behavior is determined by the crimping and undulation of the filaments before stretching and annealing with fixed ends of the textile.

The stress-strain curves in Fig. 12a show also that the elastic modulus $E$ and the tensile strength $\sigma_{max}$ of the SP60 textiles become higher after annealing and stretching them to SP60-A samples. This is explained with the orientation of the textile filaments being accompanied, as shown by the DSC and XRD data of this study, by an increase of the

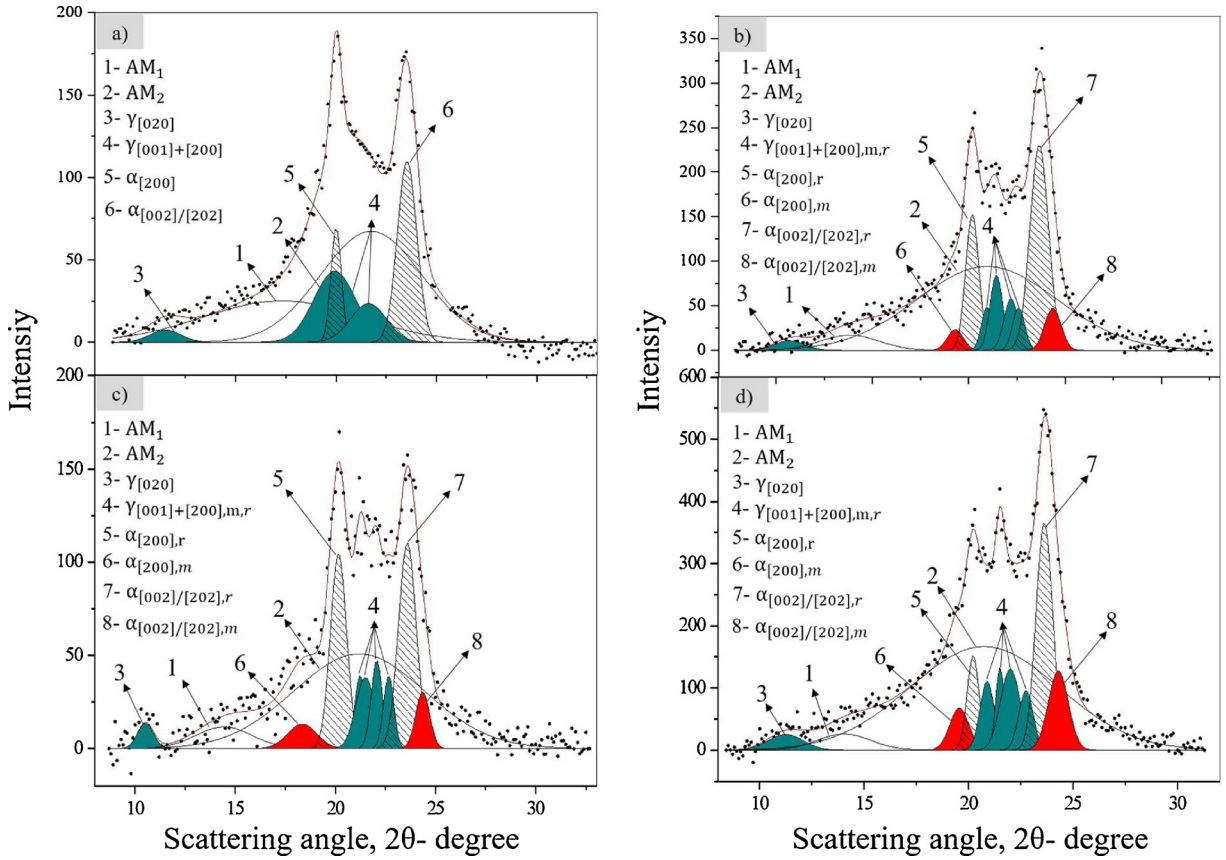


**Fig. 11.** WAXS patterns and their fits: a) anionic PA6 from EMC (PN); b) P(0)-15; c) S(0)-15; d) SP30(0)-15. The indexes **r** and **m** in the peak designations stand for Reinforcement and Matrix constituents, respectively.

**Table 5**
Data from the deconvolution of the XRD patterns of WSPC, textile structures and anionic PA6 precursors. For sample designation see Tables 1 and 2.

| Sample | α% | γ % | $X_c^{XRD}$, % | $\frac{\alpha}{\gamma}$ | $d_{\alpha(200)}$ Å | $d_{\alpha(002/202)}$ Å | $d_{\gamma(020)}$ Å | $d_{\gamma(001)}$ Å | $d_{\gamma(200)}$ Å |
|---|---|---|---|---|---|---|---|---|---|
| EMC | 26.5 | 15.2 | 41.7 | 1.74 | 4.29 | 3.62 | – | 4.31 | 3.99 |
| PN | 17.4 | 17.5 | 34.9 | 1.00 | 4.32 | 3.68 | 7.48 | 4.33 | 4.00 |
| P | 31.48 | 18.20 | 49.68 | 1.73 | 4.38 | 3.75 | 8.09 | 4.37 | 4.06 |
| P-A | 43.12 | 10.66 | 53.78 | 4.05 | 4.36 | 3.78 | 7.58 | 4.13 | 4.01 |
| P(0)-15 | $25.27^{R}$ | $8.81^{R}$ | 43.13 | 2.25 | $4.40^{R}$ | $3.76^{R}$ | 8.27 | $4.14^{R}$ | $4.00^{R}$ |
| | $4.59^{M}$ | $4.46^{M}$ | | | $4.60^{M}$ | $3.65^{M}$ | – | $4.24^{M}$ | $3.93^{M}$ |
| | **$29.86^{T}$** | **$13.27^{T}$** | | | | | | | |
| P(0)-20 | $27.68^{R}$ | $12.13^{R}$ | 52.35 | 1.93 | $4.41^{R}$ | $3.77^{R}$ | 8.20 | $4.16^{R}$ | $4.06^{R}$ |
| | $6.81^{M}$ | $5.73^{M}$ | | | $4.69^{M}$ | $3.55^{M}$ | | $4.29^{M}$ | $3.97^{M}$ |
| | **$34.49^{T}$** | **$17.86^{T}$** | | | | | | | |
| P(0)-25 | $33.63^{R}$ | $9.13^{R}$ | 51.99 | 2.37 | $4.41^{R}$ | $3.76^{R}$ | 7.28 | $4.12^{R}$ | $4.03^{R}$ |
| | $2.91^{M}$ | $6.32^{M}$ | | | $4.70^{M}$ | $3.44^{M}$ | | $4.22^{M}$ | $3.95^{M}$ |
| | **$36.54^{T}$** | **$15.45^{T}$** | | | | | | | |
| S(0)-15 | $25.84^{R}$ | $10.59^{R}$ | 48.01 | 1.93 | $4.40^{R}$ | $3.77^{R}$ | 8.40 | $4.13^{R}$ | $4.03^{R}$ |
| | $5.78^{M}$ | $5.800^{M}$ | | | $4.83^{M}$ | $3.65^{M}$ | | $4.18^{M}$ | $3.92^{M}$ |
| | **$31.62^{T}$** | **$16.39^{T}$** | | | | | | | |
| SP30(0)-15 | $17.46^{R}$ | $10.13^{R}$ | 42.55 | 1.56 | $4.39^{R}$ | $3.76^{R}$ | 7.86 | $4.13^{R}$ | $4.04^{R}$ |
| | $8.46^{M}$ | $6.500^{M}$ | | | $4.54^{M}$ | $3.66^{M}$ | | $4.25^{M}$ | $3.91^{M}$ |
| | **$25.92^{T}$** | **$16.63^{T}$** | | | | | | | |
| SP30(90)-25 | $24.62^{R}$ | $6.93^{R}$ | 45.34 | 2.02 | $4.41^{R}$ | $3.75^{R}$ | 8.21 | $4.12^{R}$ | $4.02^{R}$ |
| | $5.73^{M}$ | $8.06^{M}$ | | | $4.60^{M}$ | $3.63^{M}$ | | $4.26^{M}$ | $3.92^{M}$ |
| | **$30.35^{T}$** | **$14.99^{T}$** | | | | | | | |

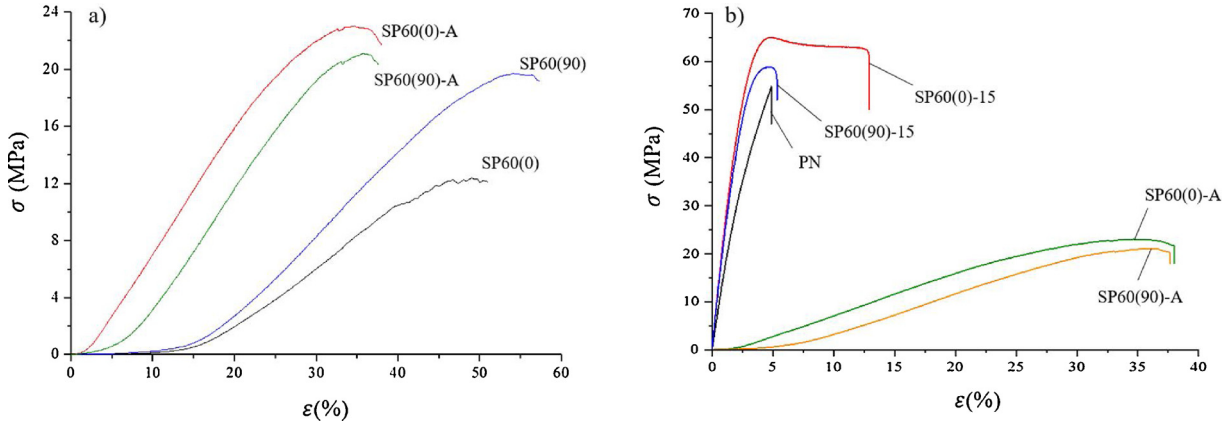


**Fig. 12.** a) Analogy of tensile behavior of stitched plain reinforcements before and after stretching-annealing treatment; b) Comparison on of stress-strain behavior of SPWSPC and the precursors. For sample designation see Tables 1 and 2.

crystallinity index and the $\frac{\alpha}{\gamma}$ ratio.

Fig.12b compares the stress-strain curves in tension of two selected stitched plain reinforced WSPC and of the respective SP reinforcements, applying the force along the two principal directions. The tensile behavior of neat isotropic PA6 matrix (PN) is shown as a reference. The latter shows a brittle failure with $\sigma_{max}$ =55 MPa at a relative deformation ε ≈ 5 %. Both stitched WSPC display similar E values whereas the $\sigma_{max}$ are higher reaching 65 MPa in the warp (0°) direction accompanied with a more ductile behavior with $\varepsilon_{max}$ = 12 %. Thus, it can be concluded that reinforcing a PA6 matrix with PA6 textile structures after appropriate mechanical and thermal treatment can improve the tensile behavior of the resulting WSPC, whereby the orientation of the plies has an important influence.

To understand the relation of the ply orientation with the mechanical properties of WSPC, the tensile characteristics $E$, $\sigma_{max}$ and $\varepsilon_{max}$ of all neat woven reinforcements were extracted from the stress-strain curves, preforming tests in both in warp (0°) and weft (90°) directions (Table 6).

Evidently, all treated reinforcement textiles used in this study display strong anisotropy of the E-modulus, the warp direction being always significantly stiffer than the weft. The *E*-values achieved after the stretching/annealing treatment were the highest for the SP30-A stitched textile. At the same time, in all textiles the strain at break values $\varepsilon_{br}$ are always larger in the weft direction. The textile reinforcements display lesser difference along the two principal directions in terms of the $\sigma_{max}$ values, and the SP60-A and P−A samples proved to be statistically isotropic in this aspect. The reason for the varying mechanical characteristics in tension of the treated textile structures is most probably related to the different possibilities for straightening of

**Table 6**
Data about the tensile properties of woven reinforcements with stretching-annealing treatment. For sample designation see Table 1.

| Specimens | Young´s modulus E (MPa) | Stress at max $\sigma_{max}$(MPa) | Strain at break $\varepsilon_{max}$(%) |
|---|---|---|---|
| P(0)-A | 21.7 ± 1.1 | 19.4 ± 1.0 | 28.1 ± 1.0 |
| P(90)-A | 3.4 ± 0.3 | 19.0 ± 1.0 | 46.2 ± 1.4 |
| S(0)-A | 43.2 ± 1.7 | 3.4 ± 0.1 | 10.0 ± 0.8 |
| S(90)-A | 1.4 ± 0.1 | 16.5 ± 1.0 | 45.1 ± 1.5 |
| SP30(0)-A | 101.1 ± 2.7 | 9.2 ± 0.5 | 26.7 ± 2.1 |
| SP30(90)-A | 7.0 ± 0.8 | 20.0 ± 0.8 | 31.1 ± 0.1 |
| SP45(0)-A | 74.8 ± 2.2 | 15.9 ± 0.6 | 28.6 ± 1.6 |
| SP45(90)-A | 2.2 ± 0.2 | 14.1 ± 0.4 | 35.7 ± 1.2 |
| SP60(0)-A | 85.8 ± 2.1 | 23.2 ± 0.1 | 17.1 ± 0.3 |
| SP60(90)-A | 3.7 ± 0.3 | 22.4 ± 1.2 | 37.5 ± 2.4 |

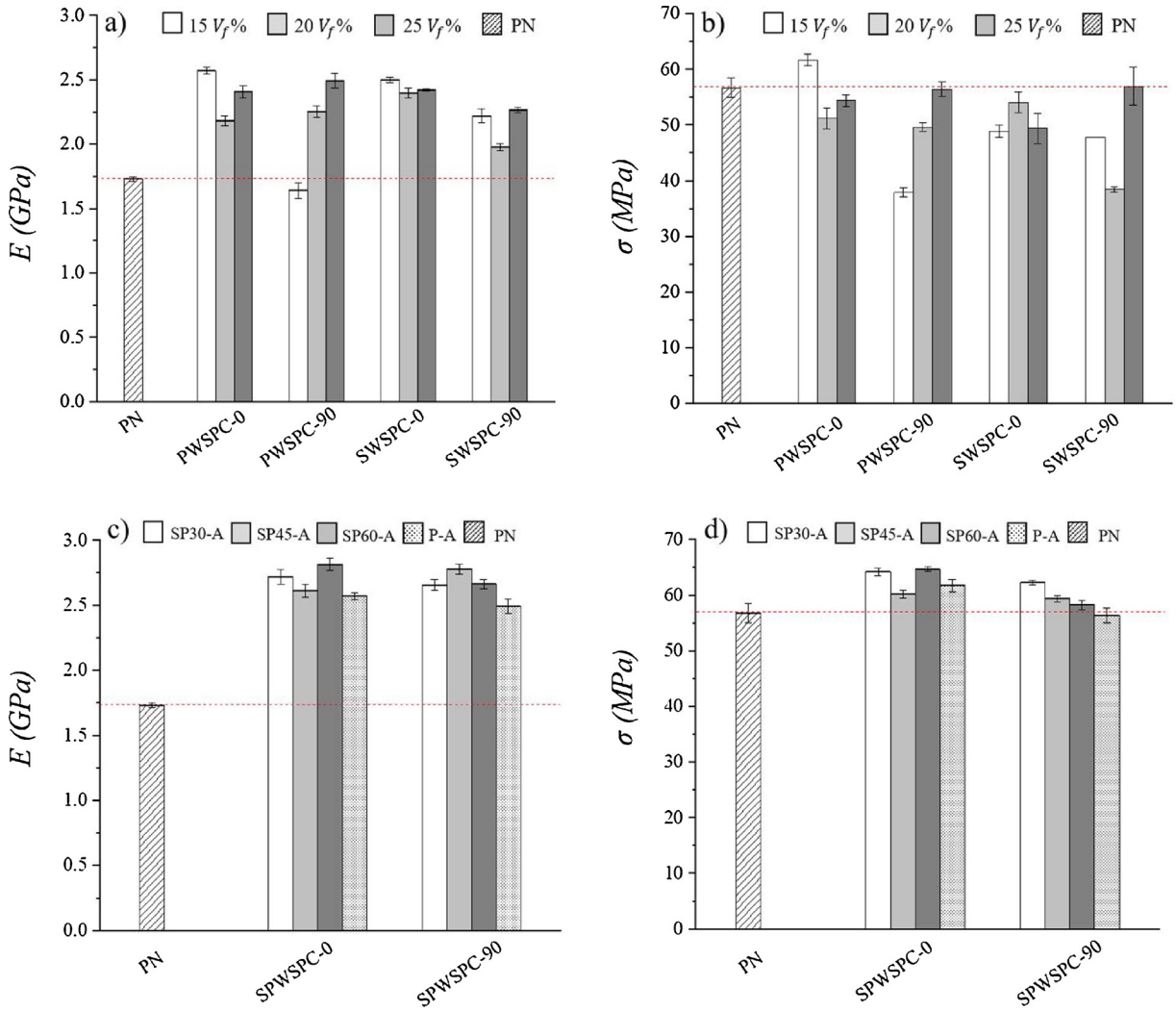


**Fig. 13.** Comparison on a) elastic modulus (E) and b) tensile strength ($\sigma$) of WSPC in relation with the reinforcement´s architectures (plain and satin) and orientation as well as fiber content. Analogical study on c) elastic modulus (E) and d) tensile strength ($\sigma$) of WSPC reinforced with stitched plain structures and orientated into two principal directions. The fiber content of 15 and 25 % was chosen for warp and weft wise SPWSPC respectively due to observing better tensile properties of PWSPC reinforced with similar $V_f$ in corresponding directions. The dashed horizontal line is presented as reference index. For sample designation see Table 2.

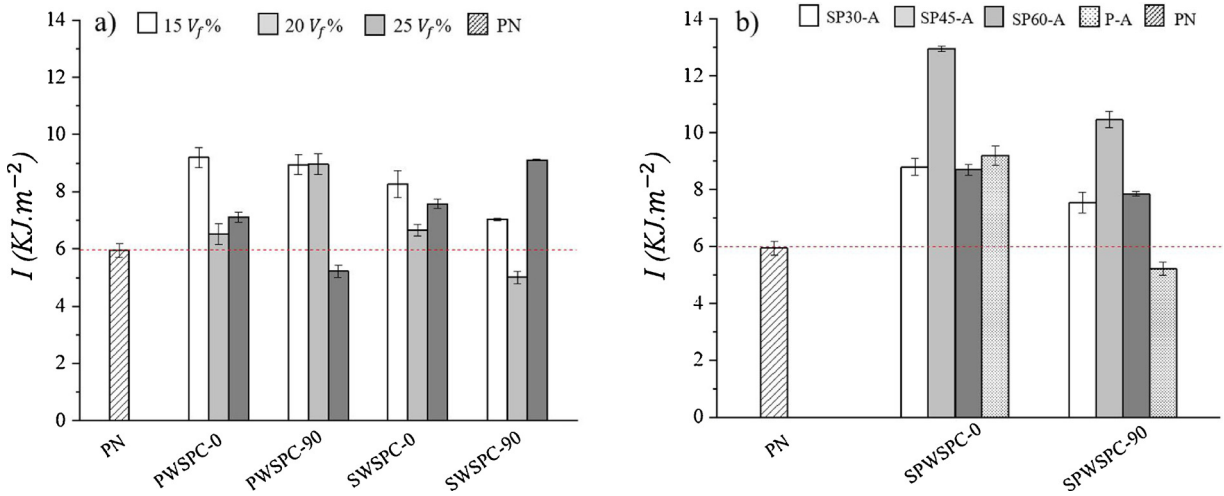


**Fig. 14.** Comparison on planar Izod Impact resistance (I) of a) WSPC reinforced with P-A and S-A structures in relation with the fiber content and test orientation; b) Analogical study on WSPC reinforced with P-A and SP-A structures with influences of fiber content, test orientation and SDF gradient. The dashed horizontal line represents reference value of the PN matrix constituents. For sample designation see Table 2.

crimped filaments and their alignment in one or other direction during the initial stretching of the textile reinforcements. Evidently, these possibilities will be dependent on the textile architecture. Notably, the novel SP−A textiles showed superior tensile characteristics in all directions.

A comparison of $E$ and $\sigma_{max}$ in tension of all WSPC is demonstrated in Fig.13a-d, as a function of the ply orientation and architecture, as well as fiber volume fractions. As seen from Fig. 13a, with the exception of PWSPC-0 sample with $V_f = 20$ %, all plain reinforced WSPC displayed $E$-values in both weft and warp directions between 2.3–2.7 GPa, i.e, higher as compared to the PA6 neat matrix (ca. 1.7 GPa), the improvement being between 40–49 %. At the same time, most WSPC demonstrated comparable or slightly lower tensile strength ($\sigma_{max}$) than that of the PN reference of ca. 57 MPa (Fig.13b). Therefore, controlling the WSPC reinforcement type, orientation and amount it is possible to produce single polymer composites with improved stiffness without deteriorating the tensile strength.

Moreover, Fig. 13c and 13d show evidence that embedment of SP-A reinforcement can produce E-values of > 2.8 GPa of the resulting WSPC in both warp and weft directions which depicts the improvement factor of 63 % in respect to the neat matrix. Meanwhile, the tensile strength of these WSPC is statistically equal or even better than that of PN, especially for WSPC reinforced with stitched plain textiles with SDF 30°.

The impact resistance ($I$) of all composites as a function of the reinforcement's architecture, test direction, $V_f$ and SDF gradient is presented in Fig. 14a-b. The $I$ value of plain and satin reinforced WSPC (Fig. 14a) is up to 55 % higher than the neat PA6 matrix. In plain-weave and satin-reinforced WSPC, there is a certain anisotropy of the impact behavior showing dependence on the $V_f$ and ply orientation. As seen from Fig. 14b, the samples containing stitched plain reinforcements (e.g. SP45(0)-15) demonstrated impact strength values with ca. 120 % higher than the PN reference. Moreover, applying stitched plain structures with 45 °SDF angle improved the impact resistance not only in respect to PN, but also as compared to other WSPC, e.g., those reinforced with P-A textile structures. The improvement is of 41 % and 102 % in warp and weft directions, respectively. The SP-A reinforced with textiles stitched at other angles showed similar impact strengths and anisotropy of the results.

### 3.6. Microstructure-mechanical properties relationship in WSPC

The main feature of the SPC is that their matrix and the reinforcements are made of the same polymer. Nevertheless, these two constituents must possess quite different, even antithetic sets of mechanical properties so as to achieve the enhanced mechanical behavior that is typical for all other composite materials. Thus, the PA6 textile filaments should be made as stiff as possible in similitude with the glass fibers in the traditional composites. As known from previous studies [38], this can be done by appropriate combined stretching and heating with fixed ends at temperatures between $T_g$ and $T_M$. On the other hand, the PA6 matrix must be ductile enough with a good adhesion at the interface with the reinforcing fibers. Comparing the WAXS data and the mechanical behavior in tension of the neat textiles (Table 5 and Fig. 12, respectively) makes evident that the enhanced mechanical resistance in tension of the annealed textile plie (e.g., the P−A sample) as compared to those without this treatment (the P-sample) is associated with a more then a twofold increase of the α-polymorph concentration in the former – from 2 to 4. This is accompanied by a very modest increase of the XRD crystallinity index from ca. 50%–54%.

After embedment the textile structure in the WSPC, the average $\frac{\alpha}{\gamma}$ ratio in the WSPC samples in Table 5 varies around 2, i.e., the α-PA6 predominates. This same ratio taken in the reinforcement PA6 of the plain-weave systems of P- and S- reinforcements is clearly higher, reaching in the case of the S(0)-15 sample its maximum of 3.73. Similar $\frac{\alpha}{\gamma}$ ratio shows also in case of SP30(90)-25 sample. It can be deduced that during the consolidation of the WSPC the textile plies maintain a relatively high content of α-PA6, which polymorph is related with higher stiffness [39–41]. At the same time, in the matrices of the WSPC where $V_f = 15$ %, $\frac{\alpha}{\gamma} \approx 1$, i.e., just like in the PN sample, suggesting a more ductile behavior [42,43]. Increasing the $V_f$ in WSPC reinforced with P-A and SP30-A leads to $\frac{\alpha}{\gamma}$ values clearly lesser than 1, meaning predominance of the γ-PA6 and increase the matrix ductility.

The mechanical properties in tension and impact are in in accordance with the microstructure of the respective WSPC. Thus, all plain-woven textiles of P-and S-type display increased E-moduli (Fig. 13a) in agreement with the increased α-PA6 in their reinforcements. Interestingly, the P-samples that possess the highest total crystallinity show a stronger anisotropy of the $E$-modulus, considering weft- and warp ply alignment. The $E$-moduli of the SP-samples were also expectedly higher having in mind the SP30(90)-25 sample polymorph content.

Similar comments on the relation between the crystalline microstructure and impact strength can be made as well. Obviously, when comparing the mechanical data of WSPC with different types of textile reinforcement one should have in mind that the geometry of the textile will be more important for the mechanical properties than the crystalline microstructure of the latter.

## 4. Conclusions

For the first time a PA6-based SPC was obtained by a two-stage process comprising: (i) powder-coating of three various PA6-based woven textile structures with previously synthesized anionic PA6 microparticles followed by (ii) consolidation of the composite by compression molding. Two conventional woven (plain and satin) and one novel stitched woven structure were applied as reinforcements, being previously stretched and annealed with fixed ends to modify appropriately their crystalline structure and orientation.

Based on SEM results, a transcrystalline layer was postulated at the reinforcement/matrix interface in all WSPC with an average thickness of 1.0–2.5 μm. The DSC and WAXS experiments proved the coexistence of α- and γ-PA6 polymorphs in all WSPC samples, whereby some variations in the crystallinity index, the polymorph ratio in either matrix or reinforcement constituents were established as the type, amount and orientation of the textile structure was changed.

The tensile properties and impact properties of PA6 based-WSPC were studied in relation with the reinforcement architecture, fiber content, reinforcement orientation. The results showed that use of the novel plain woven textiles with diagonal stitches (the SP samples) produced the best results as reinforcements in both mechanical tests characterized also by low anisotropy. It can be concluded that the technology for WSPC preparation proposed in this work can appropriately manipulate the crystalline structure of the anionic PA6 matrix and hydrolytic PA6 reinforcements so as to achieve reinforcement effect in of the Young modulus and impact properties that could be industrially relevant whenever full recycling is necessary.

## Data availability statement

The raw/processed data required to reproduce these findings cannot be shared at this time due to legal or ethical reasons.

## Declaration of Competing Interest

The authors declare that they have no known competing financial interests or personal relationships that could have appeared to influence the work reported in this paper.

## Acknowledgements

All authors gratefully acknowledge the support of the project TSSiPRO-NORTE-01-0145-FEDER-000015 funded by the regional operational program NORTE 2020, under the PORTUGAL 2020 Partnership Agreement, through the European Regional Development Fund. The partial support by FEDER funds through the COMPETE program and by national funds through FCT – Foundation for Science and Technology within the project POCI-01-0145-FEDER-007136is also acknowledged. S. D. Tohidi acknowledges FCT for the financial support through the project SFRH/BD/94759/2013. Moreover, the first author thanks for the financial support of the European Regional Development Fund (ERDF), through the operational program for COMPETE 2020 and by FCT within the project PTDC/EMEEME/30967/2017 and NORTE-0145-FEDER-030967. Additionally, N. Dencheva is also grateful for the financial support of FCTin the frames of the strategic project UID/CTM/50025/2013 and the personal program-contract CTTI-51/18-IPC.

## Appendix A. Supplementary data

Supplementary material related to this article can be found, in the online version, at doi:https://doi.org/10.1016/j.mtcomm.2020.100912.

## References

[1] R. Li, D. Yao, Preparation of single poly(lactic acid) composites, J. Appl. Polym. Sci. 107 (2008) 2909–2916.
[2] J. Karger-Kocsis, T. Bárány, Single-polymer composites (SPCs): status and future trends, Compos. Sci. Technol. 92 (2014) 77–94.
[3] D. Yao, R. Li, P. Nagarajan, Single-polymer composites based on slowly crystallizing polymers, Polym. Eng. Sci. 46 (2006) 1223–1230.
[4] F.P. La Mantia, D. Curto, R. Scaffaro, Recycling of dry and wet polyamide 6, J. Appl. Polym. Sci. 86 (2002) 1899–1903.
[5] P.J. Hine, A. Astruc, I.M. Ward, Hot compaction of polyethylene naphthalate, J. Appl. Polym. Sci. 93 (2004) 796–802.
[6] K.P. Matabola, A.R. Vries, F.S. Moolman, A.S. Luyt, Single polymer composites: a review, J. Mater. Sci. 44 (2009) 6213–6222.
[7] A. Izer, T. Bárány, Hot consolidated all-PP composites from textile fabrics composed of isotactic PP filaments with different degrees of orientation, Express Polym. Lett. 1 (2007) 790–796.
[8] M.I. Kohan, Nylon Plastics Handbook, Hanser Publishers, Cincinnati, 1995.
[9] Á. Kmetty, T. Bárány, J. Karger-Kocsis, Self-reinforced polymeric materials: a review, Prog. Polym. Sci. 35 (2010) 1288–1310.
[10] S. Fakirov, Nano- and microfibrillar single-polymer composites: a review, Macromol. Mater. Eng. 298 (2013) 9–32.
[11] F.V. Lacroix, M. Werwer, K. Schulte, Solution impregnation of polyethylene fibre/polyethylene matrix composites, Compos. Part A Appl. Sci. Manuf. 29 (1998) 371–376.
[12] Y. Gong, G. Yang, Single polymer composites by partially melting recycled polyamide 6 fibers: preparation and characterization, J. Appl. Polym. Sci. 118 (2010) 3357–3363.
[13] B. Alcock, N.O. Cabrera, N.-M. Barkoula, Z. Wang, T. Peijs, The effect of temperature and strain rate on the impact performance of recyclable all-polypropylene composites, Compos. Part B Eng. 39 (2008) 537–547.
[14] P. Dubois, O. Coulembier, J.-M. Raquez, Handbook of Ring-opening Polymerization, John Wiley & Sons, Weinheim, 2009.
[15] Y. Gong, A. Liu, G. Yang, Polyamide single polymer composites prepared via in situ anionic polymerization of ε-caprolactam, Compos. Part A Appl. Sci. Manuf. 41 (2010) 1006–1011.
[16] N. Dencheva, Z. Denchev, A.S. Pouzada, A.S. Sampaio, A.M. Rocha, Structure–properties relationship in single polymer composites based on polyamide 6 prepared by in-mold anionic polymerization, J. Mater. Sci. 48 (2013) 7260–7273.
[17] N. Dencheva, A.S. Sampaio, F.M. Oliveira, A.S. Pouzada, A.M. Brito, Z. Denchev, Preparation and properties of polyamide-6-based thermoplastic laminate composites by a novel in-mold polymerization technique, J. Appl. Polym. Sci. 131 (2014) 40083–40094.
[18] N. Dencheva, D. Vale, Z. Denchev, Dually reinforced all-polyamide laminate composites via microencapsulation strategy, Polym. Eng. Sci. 57 (2017) 806–820.
[19] I.M. Ward, P.J. Hine, The science and technology of hot compaction, Polymer (Guildf). 45 (2004) 1413–1427.
[20] D. Bhattacharyya, P. Maitrot, S. Fakirov, Polyamide 6 single polymer composites, Express Polym. Lett. 3 (2009) 525–532.
[21] S.D. Tohidi, A.M. Rocha, N.V. Dencheva, Z. Denchev, Single polymer laminate composites by compression molding of knitted textiles and microparticles of polyamide 6: preparation and structure-properties relationship, Compos. Part A Appl. Sci. Manuf. 109 (2018) 171–183.
[22] S.D. Tohidi, A.M. Rocha, N.V. Dencheva, Z. Denchev, Microstructural-mechanical properties relationship in single polymer laminate composites based on polyamide 6, Compos. Part B Eng. 153 (2018) 315–324.
[23] N. Dencheva, Z. Denchev, S. Lanceros-Méndez, T. Ezquerra Sanz, One-step in situ synthesis of polyamide microcapsules with inorganic payload and their transformation into responsive thermoplastic composite materials, Macromol. Mater. Eng. 301 (2016) 119–124.
[24] A.B. Strong, Fundamentals Of Composites Manufacturing: Materials, Methods And Applications, Society of Manufacturing Engineers, Michigan, 2008.
[25] G. Rusu, K. Ueda, E. Rusu, M. Rusu, Polyamides from lactams by centrifugal molding via anionic ring-opening polymerization, Polymer (Guildf). 42 (2001) 5669–5678.
[26] Y.P. Khanna, W.P. Kuhn, Measurement of crystalline index in nylons by DSC: complexities and recommendations, J. Polym. Sci. Part B: Polym. Phys. 35 (1997) 2219–2231.
[27] N. Dencheva, T. Nunes, M.J. Oliveira, Z. Denchev, Microfibrillar composites based on polyamide/polyethylene blends. 1. Structure investigations in oriented and isotropic polyamide 6, Polymer (Guildf) 46 (2005) 887–901.
[28] H. Quan, Z.-M. Li, M.-B. Yang, R. Huang, On transcrystallinity in semi-crystalline polymer composites, Compos. Sci. Technol. 65 (2005) 999–1021.
[29] N. Dencheva, A. Stribeck, Z. Denchev, Nanostructure development in multi-component polymer systems characterized by synchrotron X-ray scattering, Eur. Polym. J. 81 (2016) 447–469.
[30] N. Dencheva, Z. Denchev, N. Stribeck, M. Motovilin, A. Zeinolebadi, S.S. Funari, S. Botta, Nanostructure Transitions and Their Relation to Mechanical Properties in Polyethylene/P olyamide 6 Microfibrillar Composites as Revealed by SAXS/S training Studies, Macromol. Mater. Eng. 298 (2013) 1100–1116.
[31] N. Dencheva, Z. Denchev, M.J. Oliveira, S.S. Funari, Microstructure studies of in situ composites based on polyethylene/polyamide 12 blends, Macromolecules. 43 (2010) 4715–4726.
[32] Z. Denchev, N. Dencheva, S.S. Funari, M. Motovilin, T. Schubert, N. Stribeck, Nanostructure and mechanical properties studied during dynamical straining of microfibrillar reinforced HDPE/PA blends, J. Polym. Sci. Part B: Polym. Phys. 48 (2010) 237–250.
[33] S.D. Tohidi, A.M. Rocha, N. Dourado, M. Rezazadeh, N.T. Quyền, A. Zille, S. Hesseler, T. Gries, N.V. Dencheva, Z. Denchev, Influence of transcrystalline layer on finite element mesoscale modeling of polyamide 6 based single polymer laminate composites, Compos. Struct. 232 (2020) 111555.
[34] H.R. Kricheldorf, Z. Denchev, Interchange reactions in condensation polymers and their analysis by NMR spectroscopy, Transreactions Condens. Polym., Stoyko Fakirov. Transreactions in Condensation Polymers. German, Wiley-VCH, 1999, pp. 1–78.
[35] S.D. Tohidi, A.M. Rocha, N.V. Dencheva, A.S. Pouzada, Z. Denchev, Comparative structural and mechanical studies on polyamide 6 knitted-reinforced single polymer composites prepared by different reactive processing techniques, Polym. Compos. 40 (2019) 886–897.
[36] N. Dencheva, T. Nunes, M.J. Oliveira, Z. Denchev, Microfibrillar composites based on polyamide/polyethylene blends. 1. Structure investigations in oriented and isotropic polyamide 6, Polymer (Guildf) 46 (2005) 887–901.
[37] J.M. Samon, J.M. Schultz, B.S. Hsiao, Study of the cold drawing of nylon 6 fiber by in-situ simultaneous small-and wide-angle X-ray scattering techniques, Polymer (Guildf). 41 (2000) 2169–2182.
[38] N. Dencheva, Z. Denchev, M.J. Oliveira, S.S. Funari, Relationship between crystalline structure and mechanical behavior in isotropic and oriented polyamide 6, J. Appl. Polym. Sci. 103 (2007) 2242–2252.
[39] N.S. Murthy, H. Minor, C. Bednarczyk, S. Krimm, Structure of the amorphous phase in oriented polymers, Macromolecules. 26 (1993) 1712–1721.
[40] N.S. Murthy, R.G. Bray, S.T. Correale, R.A.F. Moore, Drawing and annealing of nylon-6 fibres: studies of crystal growth, orientation of amorphous and crystalline domains and their influence on properties, Polymer (Guildf). 36 (1995) 3863–3873.
[41] A. Buda, D.E. Demco, M. Bertmer, B. Blümich, V.M. Litvinov, J.P. Penning, General analytical description of spin-diffusion for a three-domain morphology. Application to melt-spun nylon 6 fibers, J. Phys. Chem. B 107 (2003) 5357–5370.
[42] L. Lin, A.S. Argon, Rate mechanism of plasticity in the crystalline component of semicrystalline nylon 6, Macromolecules. 27 (1994) 6903–6914.
[43] L. Penel-Pierron, R. Seguela, J. Lefebvre, V. Miri, C. Depecker, M. Jutigny, J. Pabiot, Structural and mechanical behavior of nylon-6 films. II. Uniaxial and biaxial drawing, J. Polym. Sci. Part B: Polym. Phys. 39 (2001) 1224–1236.